JMEPEG (2010) 19:294–300
DOI: 10.1007/s11665-009-9491-x

1059-9495/$19.00

Analysis of Microstructure and Properties of Cemented Carbide and Invar Alloy Weldment

P.Q. Xu and X.J. Zhao

(Submitted September 29, 2008; in revised form March 31, 2009)

Multi-phase composite microstructure was designed in a $Ni_{42}C_{0.6}Mn_{3.5}Nb_3Fe_{50.9}$ invar alloy which was welded to WC-Co cemented carbide. The multi-component composition ($Ni_{42}C_{0.6}Mn_{3.5}Nb_3Fe_{50.9}$) was chosen such that on welding of the cemented carbide to invar alloy the nonequilibrium interface reactions were suppressed. The microstructures of $Ni_{42}C_{0.6}Mn_{3.5}Nb_3Fe_{50.9}$ invar alloy and the dissimilar materials (WC-Co and $Ni_{42}C_{0.6}Mn_{3.5}Nb_3Fe_{50.9}$) welded joint were characterized with SEM and EDS analysis, and phase was done using x-rays diffractometer. The hardness profile is determined using micro-hardness measurements. Sound metallurgical bond and smooth hardness transition from $420HV_{0.2}$ to $870HV_{0.2}$ near interface were obtained without groove and filler materials.

Keywords cemented carbide, interface reaction, invar alloy, microstructure, phase analysis

1. Introduction

Invar alloy is a functional material with constant thermal expansion coefficient over a certain temperature range (from room temperature to 230 °C), good ductility, good weldability, excellent mechanical property, and good corrosion resistance. Therefore, it is used widely in space remote sensor, man-made satellite, precision laser measurement system, circular laser gyroscope, and waveguide. Moreover, with the development of welding techniques for invar alloy, its weldment to cemented carbide is used in liquified natural gas carrier equipment instead of stainless steel.

Welding of dissimilar materials such as cemented carbides and steel are particularly challenging because mismatches in their coefficients of thermal expansion (CTE) and thermal conductivities result in residual stress and brittle intermetallic phases (Ref 1).

Welding of cemented carbide to steel is of considerable technical interest. For example, weldments of WC-Co cemented carbide and carbon steel were obtained using braze welding (Ref 2). During this process, because of the rather large difference in the CTE of cemented carbide and carbon steel, Ag- or Cu-based soft solders were adopted to fill the welded seam. However, the low melting point of such welds cannot meet the requirement of industry.

Friction-welded joints of cemented carbide and steel with Ni as interface layer have been studied (Ref 3). Laser welding of cemented carbide and carbon steel with and without filler materials have been investigated (Ref 4, 5). To relieve the welding stress, eliminating the η carbide, preheating, postweld heat treatment, and nitridation were carried out after laser welding. The diffusion welding of cemented carbide and carbon steel have permitted complex shapes to be obtained (Ref 6). However, elemental diffusion and brittle intermetallic phases formation occur at the cemented carbide and steel interface.

Properties of Ni-based coating on cemented carbides have been studied (Ref 7). On the basis of investigation (Ref 1), we address the microstructure, composition, and mechanical properties of welded joint near WC + γ/$Ni_{42}C_{0.6}Mn_{3.5}Nb_3Fe_{50.9}$ alloy interface. First, a general discussion of the microstructure and property design strategy will be presented. The experimental procedure is described next. The microstructure, composition, phase analysis, and mechanical and physical properties of the alloys, including micro-hardness and corrosion resistance are discussed. The benefits that can be derived from addition of carbon and Nb have been highlighted.

2. Experimental

Materials to be welded were cemented carbide and invar alloy, both of which were designed via composition optimization of W-C-Co and $Ni_{42}C_{0.6}Mn_{3.5}Nb_3Fe_{50.9}$ alloys, respectively. The WC-Co cemented carbide was made by sintering with 7-μm fisher sub-sieve sizer (FSSS) WC powder and 2-μm FSSS Co binder mixture. The composition of WC-Co was 4.29%C, 65.71%W, and %Co (wt.%), and bend strength of WC-Co was 2000 MPa. The composition of invar alloy was 42%Ni, 0.6%C, 3.5%Mn, 3%Nb, and Fe (balance). The microstructure of WC-Co and invar alloy is illustrated in Fig. 1. The microstructure of WC-Co consisted of WC strengthening phase and γ phase (solid solution W or C) in Co binder. The $Ni_{42}C_{0.6}Mn_{3.5}Nb_3Fe_{50.9}$ invar alloy is illustrated in Fig. 1(b), which indicates that the microstructure contains a Ni-Fe base phase and a NbC-precipitated phase.

Materials (WC-Co and invar alloy) were cut into semi-circular shapes with no welding groove and filler materials

P.Q. Xu, School of Materials Engineering, Shanghai University of Engineering Science, Shanghai 201620, China; and **X.J. Zhao**, School of Materials Science and Engineering, Dalian Jiaotong University, Dalian 116028, China. Contact e-mails: xupeiquan7810@yahoo.com.cn and zhaoxj@djtu.edu.cn.

before welding. Welded joint of WC-Co cemented carbide to invar alloy was obtained using gas tungsten arc welding (GTAW) with double layers. The welding parameters for GTAW were welding current $I = 157$ A; welding voltage $U = 14.2$ V; welding velocity $v = 4.5$ mm/s; shield gas flow rate $L = 10$ L/min.

The microstructures and phases of the specimens were characterized by means of optical microscopy, x-ray diffraction (XRD), and scanning electron microscopy (SEM). A JSM-6360LV SEM and Electron Probe Microanalyzer EPMA-8705 equipped with an energy-dispersive spectrometer (EDS) were used for microstructure observations and composition analysis. JEM 2010 instrument was used for TEM and HRTEM observations. TEM samples were prepared using standard procedures involving ion milling. The parameters were voltage: 200 kV; Dark current: 96 μA; Emission Current: 128 μA; the current density: 109.8 pA/cm^2; explosive time: 1-8 s; and magnification is 20k× to 200k×. The samples for optical and SEM observations were etched in a solution of 1% HF, 1.5% HCl, 2.5% HNO_3, 95% H_2O, and Reagent (20% KOH + 20% K_3 [Fe $(CN)_6$] + 60% H_2O: vol.%) at room temperature.

In order to estimate the properties, Rockwell hardness (HRC) test is used to research the hardness distribution. The load is 100 kg; and the hold time is 15 s. The corrosion resistance test is carried out in 10% H_2SO_4 solution at room temperature in HH-2 type digital, constant-temperature water bath. The corrosion rate could be calculated as per the following equation:

$$v_{\text{loss}} = \frac{(m_0 - m_1)}{S \cdot t} \quad \text{(Eq 1)}$$

where, v_{loss} is corrosion rate; m_0 is mass before corrosion; m_1 is mass after corrosion; S is surface area of specimen; t is corrosion time.

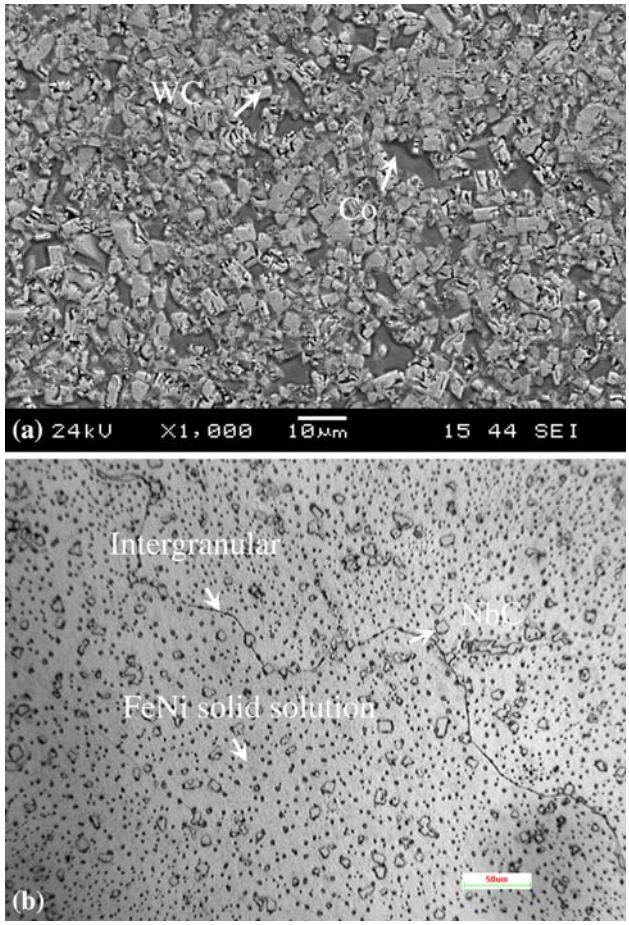

Fig. 1 Microstructure of cemented carbide and invar alloy body materials: (a) WC-Co; (b) Ni-Fe-C-Mn-Nb

3. Results

Macro image Fig. 2 of butt joint for WC-Co/$Ni_{42}C_{0.6}Mn_{3.5}Nb_3Fe_{50.9}$ invar alloy manifests a sound metallurgical bond free from faults such as porosity, fine crack, slags etc.

3.1 Microstructures

3.1.1 Composite Features of Welded Materials. Figure 3 shows the XRD trace of the $Ni_{42}C_{0.6}Mn_{3.5}Nb_3Fe_{50.9}$ invar alloy. The predominant phase identified is a fcc γ-(Fe, Ni) solid solution. The cell parameter of this solid solution phase is estimated to be 3.597 nm from the known standards. In addition to the diffraction peaks of γ-(Fe, Ni) solid solution, other peaks are present. A careful matching with known standards reveals that these peaks are from Nb_6C_5 and NbC carbide phases. We shall show later that the Nb_xC_y phase is involved in the metastable reaction, whereas some Nb_xC_y forms near grain boundary in the late stages of solidification. The XRD peaks are significantly broadened, indicating small grain/domain sizes.

Fig. 2 Macro image of WC-Co/Invar weldment

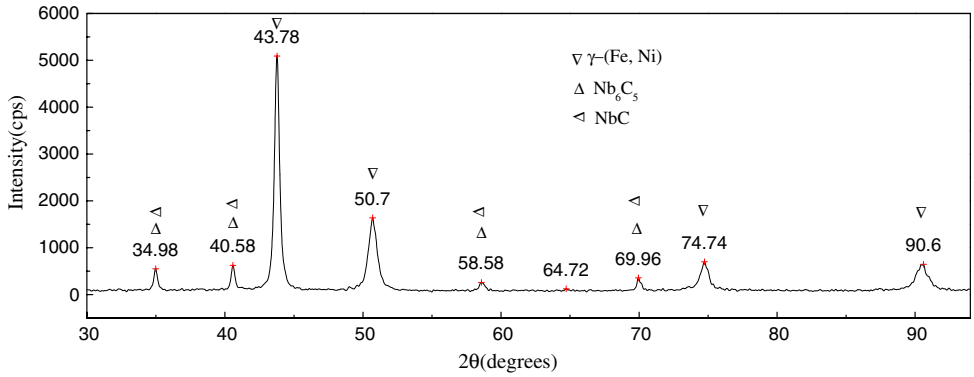

Fig. 3 XRD trace of the $Ni_{42}C_{0.6}Mn_{3.5}Nb_3Fe_{50.9}$ invar alloy

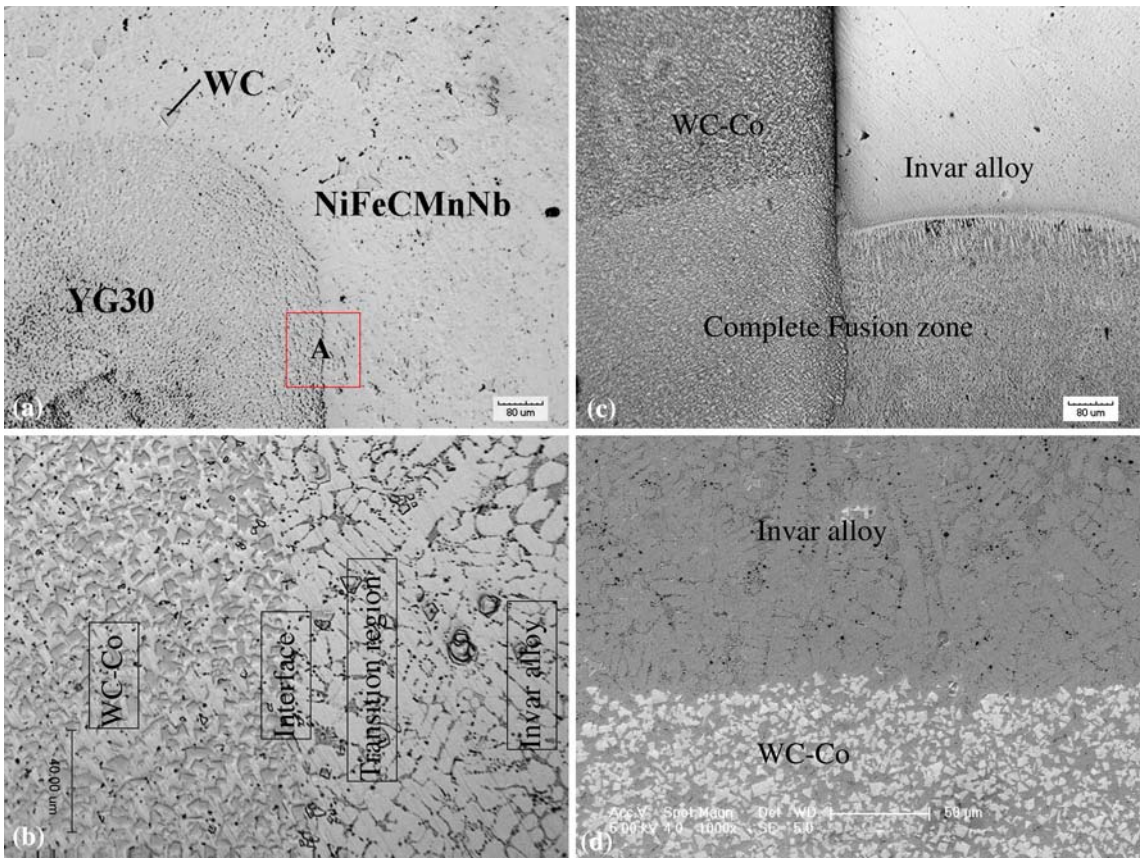

Fig. 4 SEM image and optical image of WC-Co/Invar interface, taken the cross section of the ingot: (a) Optical image at upper region; (b) Optical image at "A" region of (a); (c) bottom region; (d) SEM image of interface

SEM image and optical image of WC-Co/Invar interface obtained with the cross section of the ingot are illustrated in Fig. 4. The microstructure shows that the interface is a composite of micrometer-sized dendrites dispersed in a matrix (shown in Fig. 4a). The rounded dendrite is a few micrometers in length. The arm spacing of the dendrite is less than 5 μm. Our EDS results show that the dendritic phase is enriched in Ni, Fe, Mn, and Nb. According to XRD analysis, the dendritic phase is a γ-(Fe, Ni) (Mn, Nb) solid solution. The bulk pit morphology is shown in Fig. 4(b); the size of bulk bit is about 10 μm or so. Our EDS results show that the dendritic phase is enriched in Nb, C, or Nb and Fe. According to XRD results, the bulk phase is Nb_xC_y(Fe).

3.1.2 Composite Features of Welded Joint. Figure 5 shows the XRD trace of the high cobalt WC-Co/$Ni_{42}C_{0.6}Mn_{3.5}Nb_3Fe_{50.9}$ interface in a welded joint. The predominant phase is a fcc γ-(Fe, Ni) solid solution and WC. The cell parameter of γ-(Fe, Ni) solid solution phase is

estimated to be 3.597 nm using the known standards. In addition to the diffraction peaks of γ-(Fe, Ni) solid solution, other peaks (e.g., Nb_xC_y) are present with less amount.

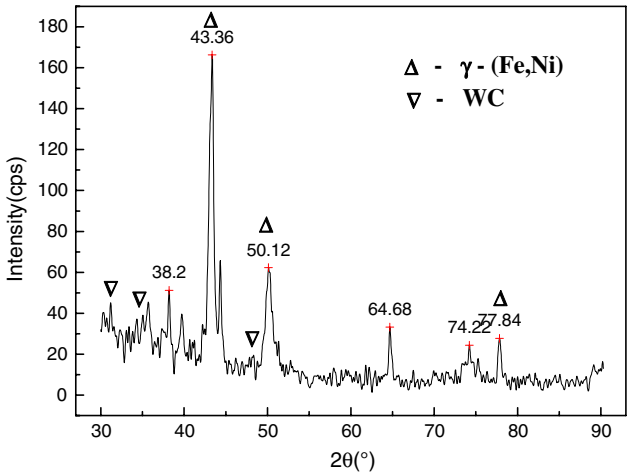

Fig. 5 XRD trace of the high cobalt WC-Co/$Ni_{42}C_{0.6}Mn_{3.5}Nb_3Fe_{50.9}$ interface in welded joint

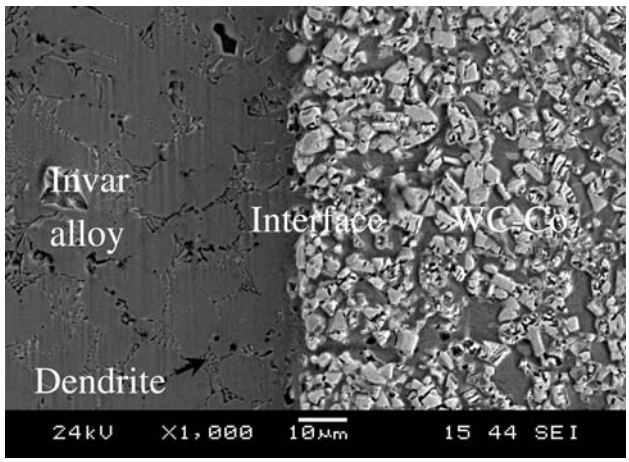

Fig. 6 SEM image of the WC-Co/$Ni_{42}C_{0.6}Mn_{3.5}Nb_3Fe_{50.9}$ interface in welded joint

SEM image of the WC-Co/$Ni_{42}C_{0.6}Mn_{3.5}Nb_3Fe_{50.9}$ interface in welded joint is shown in Fig. 6, taken near the center of the cross section of the weldment. The microstructure shows that good metallurgical bond and completely fused interface between cemented carbide and invar alloy can be obtained.

With the C and Nb addition in invar alloy, the diffusion of carbon from W-Co-C system to welded seam driven by concentration gradient of carbon is inhibited; thus, carbon depletion of W-Co-C has disappeared. Therefore, near WC-Co/$Ni_{42}C_{0.6}Mn_{3.5}Nb_3Fe_{50.9}$ interface, brittle η compound carbide is not formed.

3.2 Composition Analysis

Composition analysis for $Ni_{42}C_{0.6}Mn_{3.5}Nb_3Fe_{50.9}$ invar alloys and WC-Co/$Ni_{42}C_{0.6}Mn_{3.5}Nb_3Fe_{50.9}$ interface was investigated using EPMA-8705 analyzer.

Representative points were chosen for EDAX analysis. Figure 7 illustrates the analysis position for bulk and matrix feature. The medium-sized bulk and matrix regions are illustrated in Fig. 7(a), and their composition is shown in Table 1. The large-sized bulk and matrix are illustrated in Fig. 7(b), and the composition is shown in Table 2.

From the results, in $Ni_{42}C_{0.6}Mn_{3.5}Nb_3Fe_{50.9}$ invar alloy, middle-sized bulk is enriched in Nb and C; large-sized bulk is enriched in Fe and Nb. The matrix is enriched in Ni, Fe, and

Table 1 EDAX analysis results for spectrum from Fig. 7(a) (wt.%)

Element	Fe K	Nb L	Mn K	C	Ni
Spectrum 1	1.24	67.72	11.11	31.03	
Spectrum 2	45.24		3.42	14.24	37.10

Table 2 EDAX analysis results for spectrum from Fig. 7(b) (wt.%)

Element	Fe K	Nb L	Mn K	C	Ni
Spectrum 1	35.14		11.11		53.75
Spectrum 2	1.79	98.21			
Spectrum 3	46.98		3.71	7.92	41.39

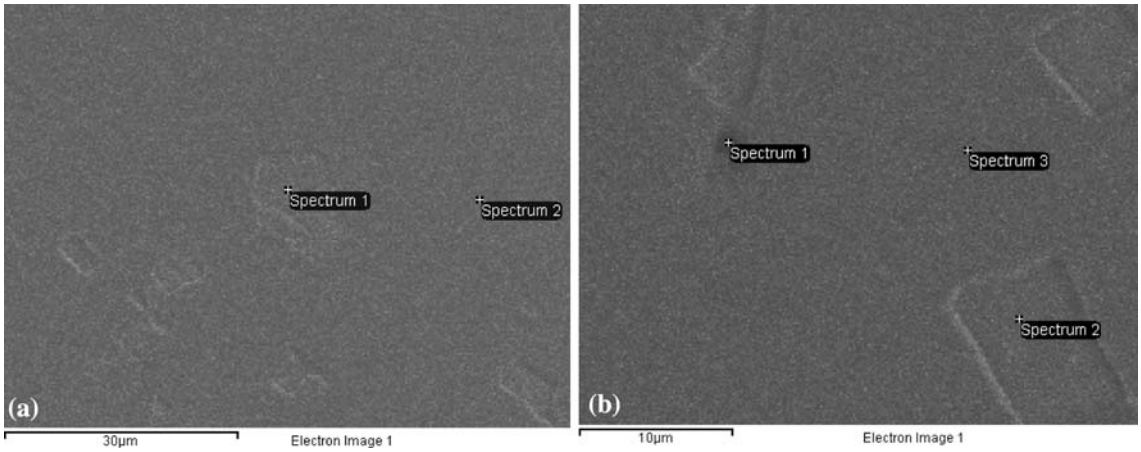

Fig. 7 Illustration of position for EDAX analysis: (a) EDAX analysis position for a serial of medium-sized bulk and matrix; (b) EDAX analysis position for large-sized bulk and matrix

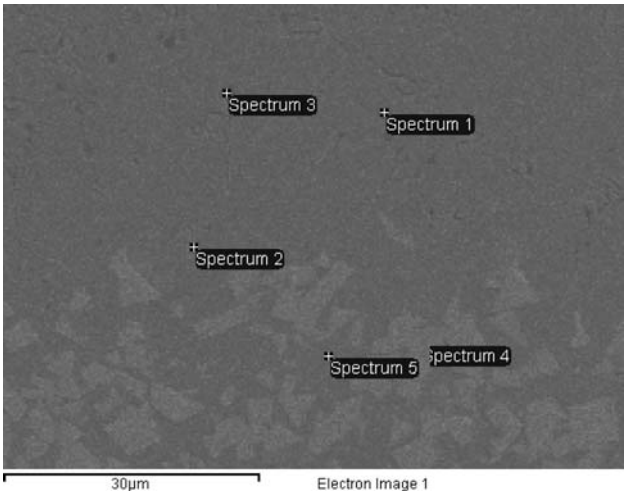

Fig. 8 Illustration of position for EDAX analysis of WC-Co/$Ni_{42}C_{0.6}Mn_{3.5}Nb_3Fe_{50.9}$ interface

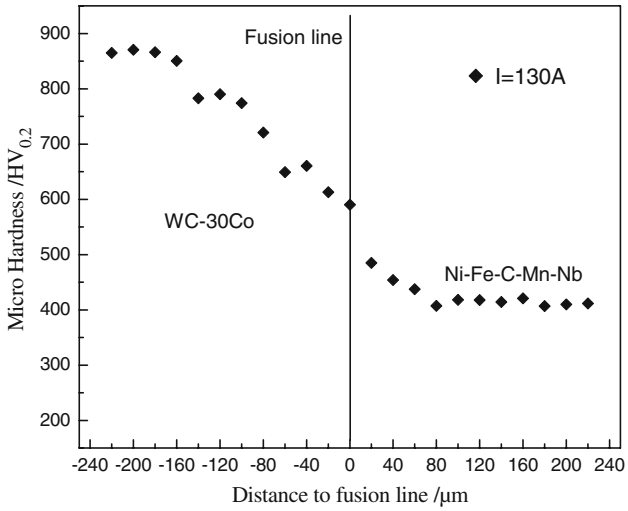

Fig. 9 Micro-hardness distribution on near WC-Co/$Ni_{42}C_{0.6}Mn_{3.5}Nb_3Fe_{50.9}$ interface

Table 3 EDAX analysis results for spectrum from Fig. 8 (wt.%)

Element	Fe K	W L	Mn K	C	Ni	Co	Nb
Spectrum 1	38.56	10.11	2.23	6.68	34.08	8.35	
Spectrum 2	26.49	26.05	1.88	6.74	21.53	5.74	11.57
Spectrum 3	37.70	10.20	2.46	7.31	33.85	8.48	
Spectrum 4	1.05	85.03		13.93			
Spectrum 5	34.05	12.47	1.87	13.88	28.31	9.42	

Table 4 The macro-hardness distribution near WC-Co/ welded seam interface

Distance to fusion line near WC-Co side, μm	Rockwell hardness, HRC
1	49.0
379	45.0
687	43.3
885	36.7
1768	16.3

Mn. The results manifest that the bulk might be NbC or NbFe through the reaction of Nb, Fe, and C. The matrix might be (Fe, Ni) solution. According to further x-ray analysis results, the matrix might be γ-(Ni, Fe) solution.

In order to determine the composition near WC-Co/$Ni_{42}C_{0.6}Mn_{3.5}Nb_3Fe_{50.9}$ interface, typical points near the interface are chosen for EDAX analysis. Figure 8 illustrates the analysis position for bulk and matrix features, and their composition is shown in Table 3.

From the results, near WC-Co/$Ni_{42}C_{0.6}Mn_{3.5}Nb_3Fe_{50.9}$ invar alloy interface, white bulk is enriched in W and C. The matrix is enriched in Fe, Ni, and might be (Fe, Ni) solution. According to further x-ray analysis results, the composition might be γ-(Ni, Fe) solution and WC.

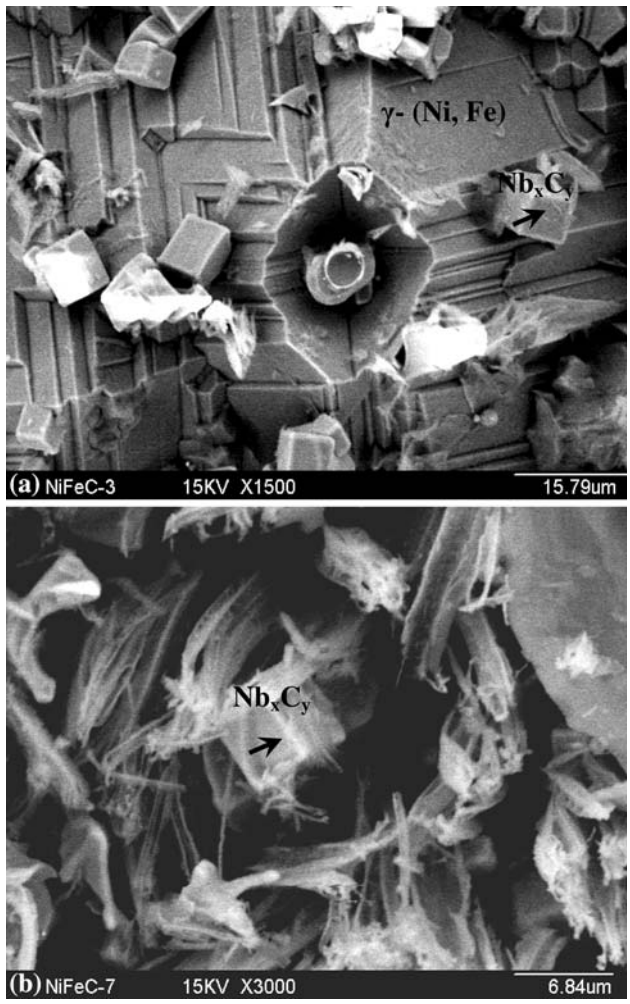

Fig. 10 SEM image of $Ni_{42}C_{0.6}Mn_{3.5}Nb_3Fe_{50.9}$ invar alloy after corrosion in 10% H_2SO_4 solution: (a) Microstructure distribution; (b) Morphology of Nb_xC_y

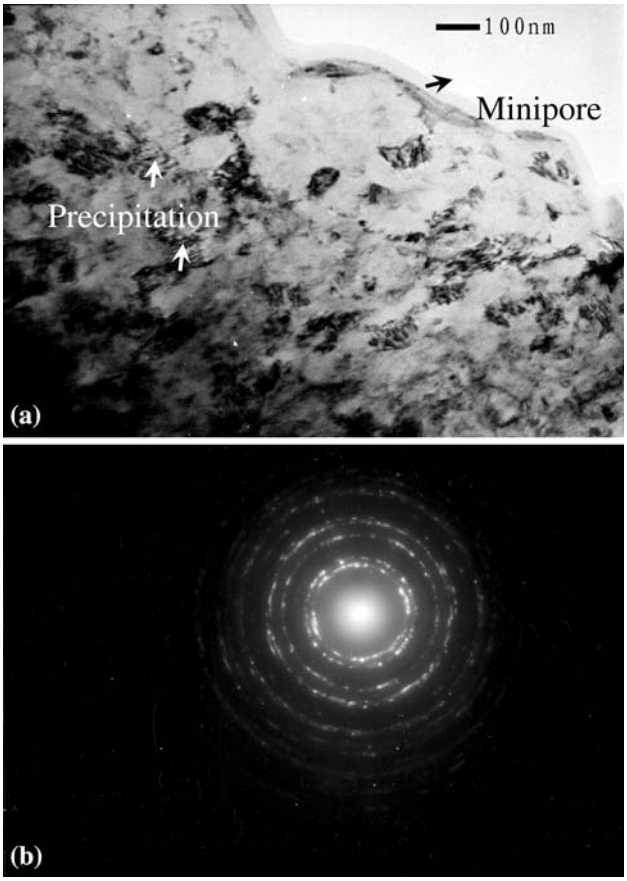

Fig. 11 TEM image of near invar alloy at interface: (a) TEM images showing the precipitation and its (b) SAED patterns

3.3 Hardness Distribution and Corrosion Resistance

In order to estimate the property of butt joint of WC-Co to NiFeCMnNb invar alloy, macro hardness distribution was determined, and the results of HRC distribution are illustrated in Table 4. There is about 1-mm wide transition region where Rockwell hardness varies from 49 HRC to 16.3 HRC.

In order to confirm there were no η phases near interface, we carried out micro-hardness test. After polishing, HXD-1000 type micro-hardness tester was used to investigate the micro-hardness distribution near WC-Co/$Ni_{42}C_{0.6}Mn_{3.5}Nb_3Fe_{50.9}$ interface. The results are illustrated in Fig. 9. From the profile, micro-hardness of WC-Co ($870HV_{0.2}$) was much higher than that of invar alloy ($420HV_{0.2}$). The micro-hardness of welded seam is nearly $460\text{-}600HV_{0.2}$. A smooth curve of micro-hardness was achieved from welded seam to WC-Co which manifested that no η phase had formed near WC-Co/$Ni_{42}C_{0.6}Mn_{3.5}Nb_3Fe_{50.9}$ interface. Moreover, the smooth hardness profile indicated good metallurgical bond across the whole butt joint. The micro-hardness test results agree with the microstructure analysis, composition analysis, and x-ray analysis.

Figure 10(a) shows the microstructure of $Ni_{42}C_{0.6}Mn_{3.5}Nb_3Fe_{50.9}$ invar alloy after corrosion, and Fig. 10(b) shows the strengthening particle morphology. The corrosion velocity v_{loss} is 8 g/m^2 h^1. As can be inferred from the microstructure distribution and morphology, the corrosion resistance is mainly attributed to the γ-(Ni, Fe) solution.

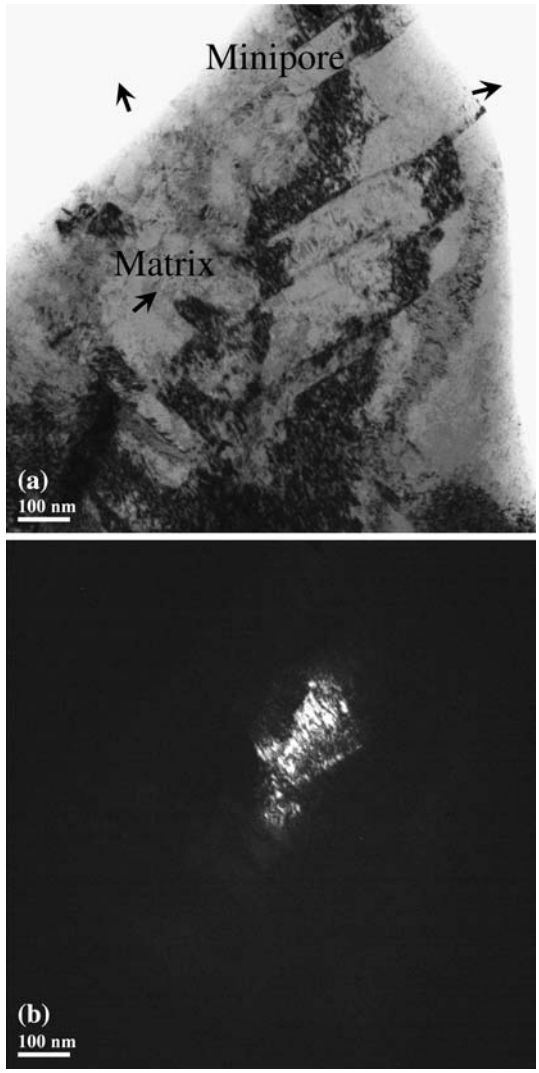

Fig. 12 TEM image of bright-field and dark-field: (a) Bright-field TEM images of the matrix observed and (b) its corresponding dark-field image

3.4 TEM Analysis

The TEM images of the matrix and the precipitation are illustrated in Fig. 11 and 12, respectively. Figure 11(a) shows the TEM images of the precipitation, and Fig. 11(b) shows their SAED patterns. From the results, we can see that the precipitation forms in matrix, and the precipitate size is small. Figure 12(a) shows the bright-field TEM images of the matrix, and Fig. 12(b) shows its corresponding dark-field image. The results indicate that the precipitation might be the black NbC phase.

4. Summary

(1) Sound metallurgical bond between WC-Co and NiFeCMnNb invar alloys can be obtained by using a

fusion welding method. The addition of Nb improved the hardness of invar alloy by forming NbC and FeNb near grain boundary.

(2) The main phases consist of γ-(Fe, Ni) solution, WC, and NbC. The higher micro hardness is contributed by strengthening due to NbC and WC dispersion.

Acknowledgments

The authors acknowledge the support extended by Shanghai Educational Development Foundation (2008cg62), Specialized Research Fund for Excellent Teachers of Shanghai (06xpyq17), National Natural Science Foundation of China (50775135), and Shanghai Leading Academic Discipline Project (J51402). Special thanks are also due to Prof. Shun Yao from Welding Engineering Institute, Shanghai Jiao Tong University; L.N. Li from Dalian Jiaotong University; Y.J. Xue, Z. Huang, L.W. Zhang, and Y.W. Xu from Shanghai University of Engineering Science.

References

1. P.Q. Xu, D.X. Yang, X.J. Zhao, and S. Yao, Novel Weld Material (Ni-Fe-C) for GTA Welding of WC-Co to 45 Carbon Steel, *J. Mater. Sci.*, 2005, **40**, p 6559–6564
2. W. Lee, B. Kwon, and S. Jung, Effect of Cr_3C_2 on the Microstructure and Mechanical Properties of the Brazed Joints WC-Co and Carbon Steel, *Int. J. Refract. Met. Hard Met.*, 2006, **24**, p 215–221
3. M. Shamanian, M. Salehi, and A. Saatchi, et al., Influence of Ni Interlayers on the Mechanical Properties of WC-Co Friction Welds, *Mater. Manuf. Process.*, 2003, **18**, p 581–598
4. C. Barbatti, J. Garcia, and G. Liedl, et al., Joining of Cemented Carbides to Steel by Laser Beam Welding, *Materialwiss. Werkst.*, 2007, **38**, p 907–914
5. A. Costa, L. Quintino, and M. Miranda, Microstructural Aspects of Laser Dissimilar Welds of Hard Metals to Steels, *J. Laser Appl.*, 2004, **16**, p 206–211
6. H. Masumoto, K. Nishio, and H. Matuda, Diffusion Bonds Between Tungusten or Cemented Carbide and Stainless Steel, *Pre-Prints Natl Meet. JWS*, 2004, **174**, p 144–145
7. H. Kim, S. Hwang, and C. Lee, et al., Assessment of Wear Performance of Flame Sprayed and Fused Ni-based Coatings, *Surf. Coat. Technol.*, 2003, **172**, p 262–269